Acta Pharmaceutica Sinica B 2020;10(8):1549−1562

Chinese Pharmaceutical Association
Institute of Materia Medica, Chinese Academy of Medical Sciences

Acta Pharmaceutica Sinica B

www.elsevier.com/locate/apsb
www.sciencedirect.com

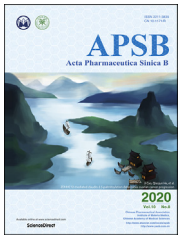

ORIGINAL ARTICLE

A magnetism/laser-auxiliary cascaded drug delivery to pulmonary carcinoma

Jialiang Lin[a], Qingqing Yin[a], Binlong Chen[a], Haoran Zhang[a], Dong Mei[a], Jijun Fu[c], Bing He[a], Hua Zhang[a], Wenbing Dai[a], Xueqing Wang[a], Yiguang Wang[a], Qiang Zhang[a,b,*]

[a]*Beijing Key Laboratory of Molecular Pharmaceutics and New Drug Delivery Systems, School of Pharmaceutical Sciences, Peking University, Beijing 100191, China*
[b]*State Key Laboratory of Natural and Biomimetic Drugs, Peking University, Beijing 100191, China*
[c]*School of Pharmaceutical Science, Guangzhou Medical University, Guangzhou 511436, China*

Received 12 September 2019; received in revised form 8 November 2019; accepted 30 November 2019

KEY WORDS

USPIONs;
c(RGDfK);
Laser-heating;
Magnetic targeting;
Streptavidin−biotin;
Lipid nanosystem

Abstract Although high-efficiency targeted delivery is investigated for years, the efficiency of tumor targeting seems still a hard core to smash. To overcome this problem, we design a three-step delivery strategy based on streptavidin−biotin interaction with the help of c(RGDfK), magnetic fields and lasers. The ultrasmall superparamagnetic iron oxide nanoparticles (USIONPs) modified with c(RGDfK) and biotin are delivered at step 1, followed by streptavidin and the doxorubicin (Dox) loaded nanosystems conjugated with biotin at steps 2 and 3, respectively. The delivery systems were proved to be efficient on A549 cells. The co-localization of signal for each step revealed the targeting mechanism. The external magnetic field could further amplify the endocytosis of USPIONs based on c(RGDfK), and magnify the uptake distinctions among different test groups. Based on photoacoustic imaging, laser-heating treatment could enhance the permeability of tumor venous blood vessels and change the insufficient blood flow in cancer. Then, it was noticed *in vivo* that only three-step delivery with laser-heating and magnetic fields realized the highest tumor distribution of nanosystem. Finally, the magnetism/laser-auxiliary cascaded delivery exhibited the best antitumor efficacy. Generally, this study demonstrated the necessity of combining physical, biological and chemical means of targeting.

*Corresponding author. Tel./fax: +86 10 82802791.
E-mail address: zqdodo@bjmu.edu.cn (Qiang Zhang).

Peer review under responsibility of Institute of Materia Medica, Chinese Academy of Medical Sciences and Chinese Pharmaceutical Association.

https://doi.org/10.1016/j.apsb.2019.12.017

1. Introduction

Currently, surgery, chemotherapy, biotherapy and radiotherapy are the most important treatments for many tumors. For decades, because the conventional chemodrugs are extremely lack of specificity, the researchers have explored a variety of approaches, such as drug delivery system[1], etc. to enhance tumor targeting. Specially, the investigations related to nanotechnology including new nanomaterials[2] and lipid-based nanoparticles[3] are among the hot topics of research. In despite of a great deal of literatures available, nanomedicine targeting tumors still faces great challenges: there are few commercial functionalized nanomedicines[4], and even few successful clinical trials related[5]. It seems an indisputable fact that a targeted system often demonstrates obvious selectivity at cell level, but fails *in vivo*[6], which are largely attributed to the complexity of tumors[7,8]. It is generally believed that a simple targeting strategy may be of great limitation in terms of efficacy and specificity, but a fancy delivery system tends to get further from reality, which seems a big issue in this field[9].

Actually, the targeting efficiency is associated with both targeted delivery system and the status of tumors[10,11]. Currently, researches focus more on the former, but less on the latter or both aspects at the same time. To address this issue, we propose a combination of different delivery mechanisms effectively with simultaneous consideration on both delivery functions and the tumor status.

Based on our observation, the blood supply to the A549 tumor tissue was less than normal site. So, raising tumor temperature may enhance permeability of tumor blood vessels and amplify the enhanced permeability and retention (EPR) effect of nanomedicine. Up to now, there are only a few reports using laser[12], heating[13,14] or microwave[15,16] to warm up the tumor tissue in order to increase tumor blood flow, but most of these do not deal with drug delivery.

Among the active targeting strategy, RGD-integrin mediation is a well-recognized approach, and among drug nanocarriers[17,18], lipid vehicles are widely utilized due to their high drug loading and biocompatibility[19,20]. The magnetism is another well-confirmed targeting strategy, and ultrasmall superparamagnetic iron oxide nanoparticles (USIONPs) are often chosen for this aim, although their drug loadings are not high[21]. Due to the very strong binding of avidin−biotin[22,23], it is used for pretargeting[24], cell probe[25], biosensor detection[26] and promotion of nanocarrier penetration to tumor tissue[27].

Generally, we develop a combination drug system for magnetism/laser-auxiliary three-step delivery based on Arg-Gly-Asp (RGD)-integrin and avidin−biotin binding. Firstly, we irradiate the tumor with a laser to elevate vascular permeability. Then, the administered USIONPs modified with RGD and biotin are expected to target to the integrin-expressed tumor, more efficiently under an applied magnetic field at tumor site. Next, the given streptavidin may combine with the biotin on the surface of functionalized USIONPs. Finally, a dose of doxorubicin (Dox) loaded lipid vehicles modified with biotin may bind with streptavidin there and exert killing by the released drug. Here, the lung carcinoma as the highest incidence and mortality of all cancers[28] is used as the tumor model.

2. Materials and methods

2.1. Experimental materials

See Supporting Information Section 1.

2.2. Preparation of the combination drug system

We used thermal decomposition method to fabricate the nonpolar USIONPs, and used DSPE-PEG2K-c(RGDfK) and DSPE-PEG2K-biotin as amphiphilic materials to package the non-polar USPIONs. Similarly, the USPIONs could also be modified with biotin, control peptide c(RADfK), rhodamine, 1,1′-dioctadecyl-3,3,3′,3′-tetramethylindodicarbocyanine (Did), 1,1′-dioctadecyl-3,3,3′,3′-tetramethylindotricarbocyanine iodide (Dir). The lipid nanosystem were prepared by film dispersion method and modified with biotin. The lipid nanosystem was also loaded with doxorubicin, or labeled with Did and Dir, respectively. Other specific preparation methods can be found in Supporting Information.

2.3. Characterizations of the combination drug systems

2.3.1. Morphology

Morphological characterization was performed using transmission electron microscopy (TEM, JEOL Ltd., Tokyo, Japan). TEM micrographs were obtained with a JEM-1200EX electron microscope, operating at 120 kV. The samples were prepared by depositing 4 μL nanoparticles dispersion in 10 μL distilled water on a carbon-coated copper grid and letting the solvent to evaporate. After the sample was dried, it was negatively stained with 2% phosphotungstic acid, and observed by TEM.

2.3.2. MALDI-TOF MS analysis

The aqueous dispersion of USIONPs modified with c(RGDfK) and biotin (2 μL) was deposited on the MALDI plate. After dried, the sample was analyzed using MALDI-TOF MS (AB SCIEX, 5800 MALDI-TOF/TOF, Boston, MA, USA).

2.3.3. Magnetic characterization

Magnetic characterization was performed with a Vibrating sample magnetometer (VSM, BKT-4500, Beijing, China). The aqueous dispersion of USIONPs modified with c(RGDfK) and biotin was freeze-dried. The product was weighed about 5 mg and wrapped in tape, placed in a VSM magnetometer and tested for M−H curve.

2.3.4. Particle size and potential measure

We took 100 μL dispersion of the USIONPs modified with c(RGDfK) and biotin, diluted it with 900 μL of pure water. We did the same for the dispersion of doxorubicin-loaded lipid nanosystem. We measured the particle size and potential of USIONPs and doxorubicin-loaded lipid nanosystem using a Malvern particle size analyzer (Malvern zetasizer Nano ZS, Malvern, UK).

2.4. Cellular uptake assay

2.4.1. Endocytosis of combination system via three-step delivery without external magnetic field

A549 cells were cultured in confocal dishes and cultivated at 37 °C until they reached 70%. The experiments were divided into 6 groups, each of which was shown in Supporting Information Table S1.

Cellular uptake of combination system *via* three-step strategy: the first step was to administer USIONPs (100 μg/mL, modified with c(RGDfK) or c(RADfK), biotin and rhodamine) and incubate for 9 h at 37 °C. After discarding the culture medium, the cells were washed 2 times with complete culture medium; the second step was to add 25 μg/mL of Andy Fluor 488 labeled streptavidin

complete medium and incubate at 37 °C for 1 h, then discard the medium and washed the cells 2 times with complete medium; in the third step, after dilution with complete culture medium, lipid nanosystem modified with biotin and marked with Did (equivalent to 0.25 μg/mL Did) was added and incubated at 37 °C for 4 h. The medium was discarded and the cells were washed twice with culture medium. Finally, the cells were fixed with 4% paraformaldehyde for 10 min at room temperature. Cell nuclei were stained with Hoechst 33,258, and the samples were observed using a Leica TCS SP8 confocal laser-scanning microscope (CLSM, Heidelberg, Germany). For the nucleus, the excitation wavelength was 405 nm and the emission wavelength was 430−470 nm. For the Andy Fluor 488, the excitation wavelength was 488 nm and the emission wavelength was 502−558 nm. For

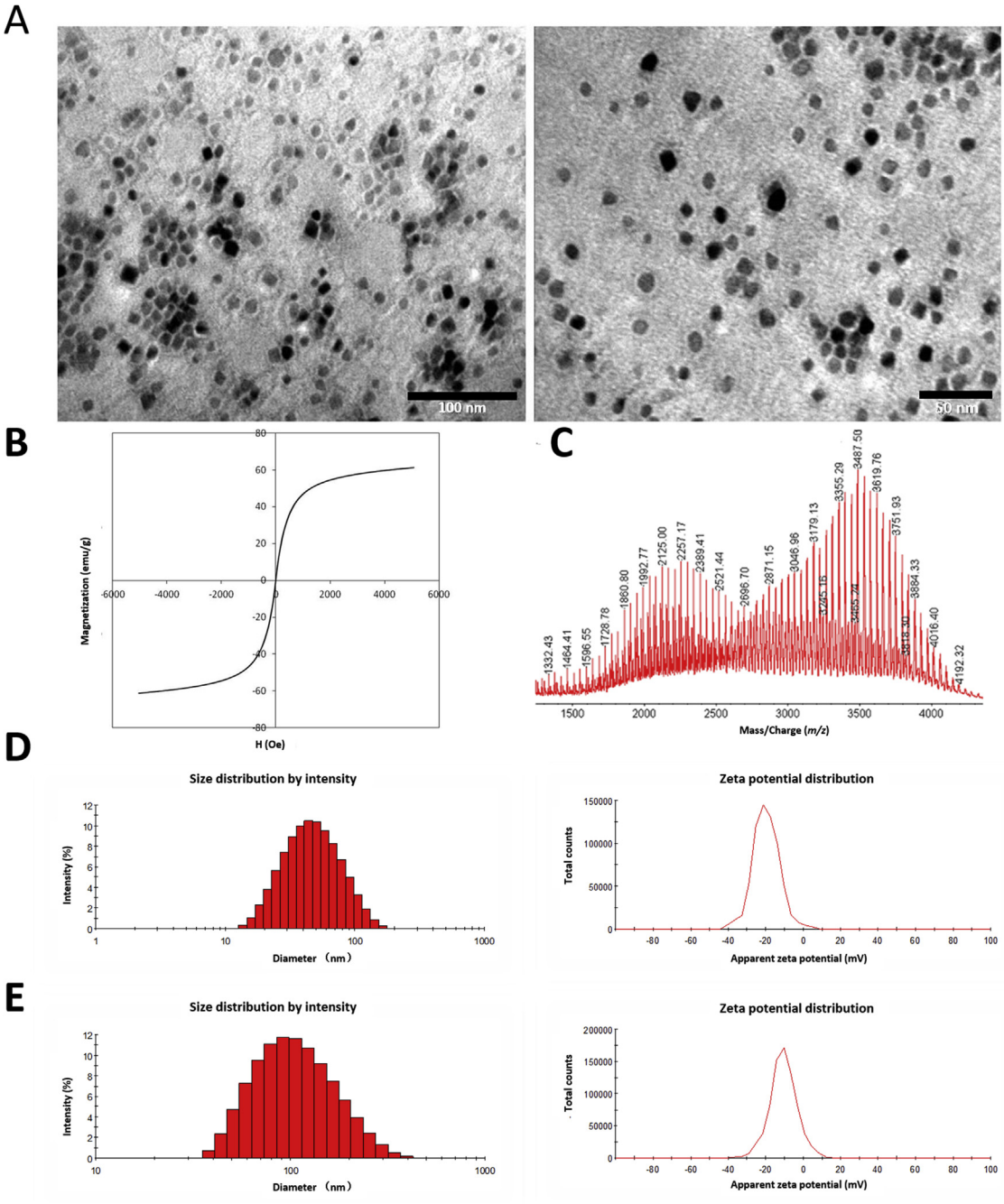

Figure 1 Characterizations of USPIONs modified with c(RGDfK) and biotin, and doxorubicin loaded lipid nanosystem modified with biotin. (A) TEM of USPIONs modified with c(RGDfK) and biotin (left: × 400,000; right: × 550,000). (B) Magnetization curve (M−H curve) of USPIONs modified with c(RGDfK) and biotin in 298K. (C) MALDI-TOF-MS of USPIONs modified with c(RGDfK) and biotin. (D) Size distribution (left) and zeta potential (right) of USPIONs modified with c(RGDfK) and biotin. (E) Size distribution (left) and zeta potential (right) of doxorubicin loaded lipid nanosystem modified with biotin.

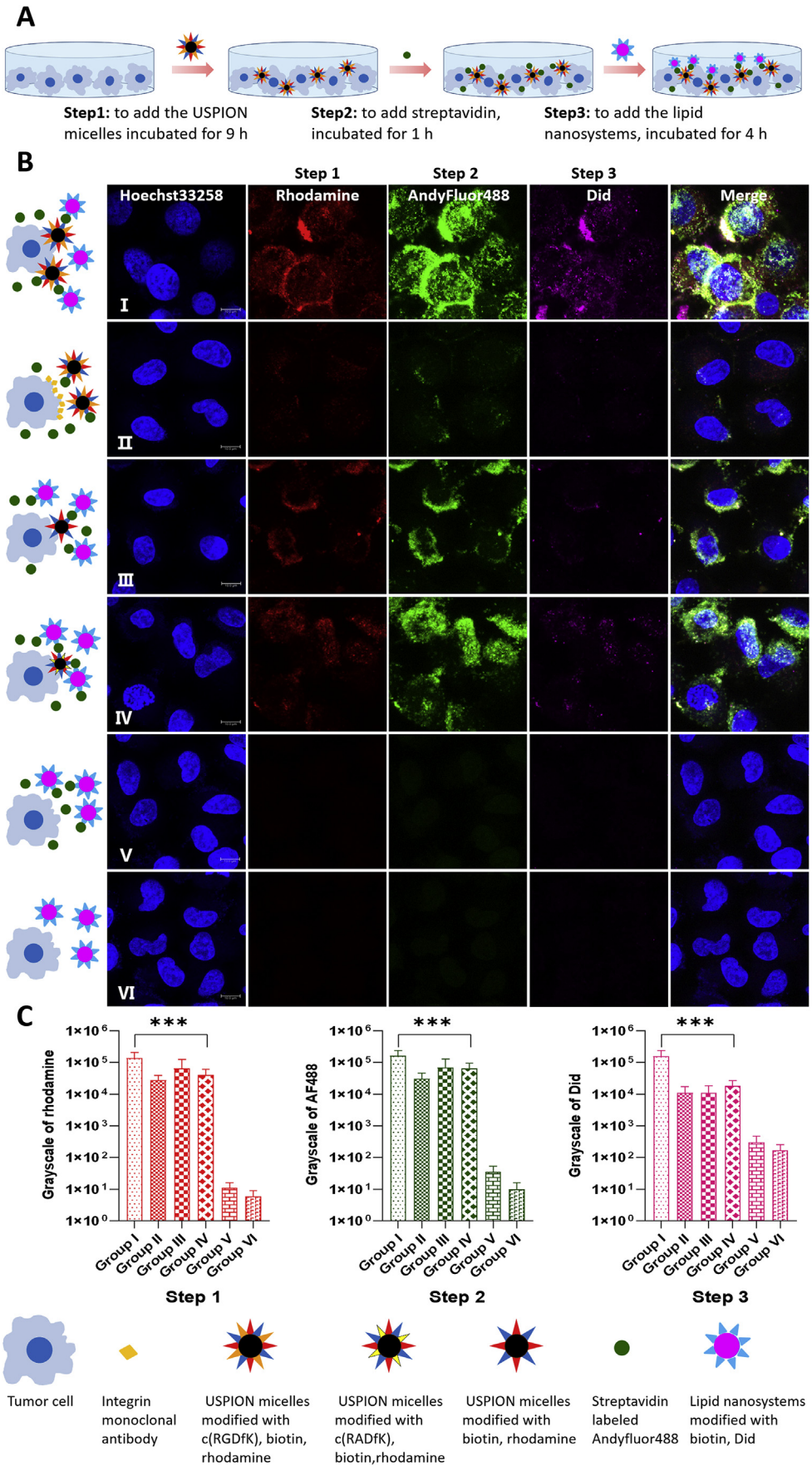
A
Step1: to add the USPION micelles incubated for 9 h
Step2: to add streptavidin, incubated for 1 h
Step3: to add the lipid nanosystems, incubated for 4 h
B
Step 1
Step 2
Step 3
Hoechst33258
Rhodamine
AndyFluor488
Did
Merge
I
II
III
IV
V
VI
C
Grayscale of rhodamine
Grayscale of AF488
Grayscale of Did
***
Group I
Group II
Group III
Group IV
Group V
Group VI
Step 1
Step 2
Step 3
Tumor cell
Integrin monoclonal antibody
USPION micelles modified with c(RGDfK), biotin, rhodamine
USPION micelles modified with c(RADfK), biotin,rhodamine
USPION micelles modified with biotin, rhodamine
Streptavidin labeled Andyfluor488
Lipid nanosystems modified with biotin, Did

the rhodamine, the excitation wavelength was 561 nm and the emission wavelength was 577−623 nm. For the Did, the excitation wavelength was 633 nm and the emission wavelength was 650−722 nm.

2.4.2. Cellular uptake of USIONPs with external magnetic field

2.4.2.1. Prussian blue staining method. A549 cells were cultured in 96-well plates and cultivated at 37 °C until reached 70%. The experiments were divided into 4 groups: USIONPs without modification; USIONPs modified with c(RADfK); USIONPs modified with c(RGDfK); USIONPs modified with c(RGDfK) and biotin. The samples were diluted to 50 μg/mL (Fe/mL) with culture medium. NdFeB permanent magnets (*Φ* 5 mm × 4 mm, 0.42 T) were placed under the 96-well plates. After incubating at 37 °C for 8 h, the cells were washed three times with PBS, and fixed with 4% paraformaldehyde for 20 min at room temperature, followed by staining with the Prussian blue solution (equal volume of 2% hydrochloric acid and 2% potassium Ferro cyanide) for 30 min. The iron staining was observed using an optical microscopy (IX81, Olympus, Tokyo, Japan).

2.4.2.2. Inductively coupled plasma mass spectrometry (ICP-MS). A549 cells were cultured in two 24-well plates at 37 °C until reached 70%. The experimental groups were divided into a magnetic field group and a non-magnetic field group. Each group was divided into 3 different sub-groups: USIONPs modified with biotin, USIONPs modified with c(RADfK) and biotin, USIONPs modified with c(RGDfK) and biotin, and blank control without USIONPs. Each sub-group was repeated four times. The amount of iron oxide nanoparticles per sample was 40 μg/well (in terms of Fe content). NdFeB permanent magnets (*Φ* 10 mm × 10 mm, 0.55 T) were placed under the 24-well plates to provide magnetic field. After incubating at 37 °C for 2 h, the cells were washed three times with PBS. Each well was added with 50 μL 1% TritonX-100 and 200 μL of pure water to digest cells at 4 °C for 30 min. The digestive solutions were transferred to 0.5 mL EP tube. The iron contents of each sample were detected by inductively coupled plasma mass spectrometry (ICP-Ms, Elan DRCII, PerkinElmer, Waltham, MA, USA), and the cellular protein contents of each sample were assayed using a Coomassie brilliant blue method at 540 nm. The results of iron content were divided by the cellular protein contents, namely the results were the amount of iron uptake per unit of cells.

2.4.3. Endocytosis of combination system via cascaded delivery with external magnetic field

A549 Cells were seeded in confocal dishes and cultivated at 37 °C until their amount reached 70%. The experiments were divided into 4 groups, each of which was shown in Supporting Information Table S3.

Cellular uptake of combination system *via* three-step strategy: the first step was to add aqueous dispersion of rhodamine labelled USIONPs (Fe, 10 μg/dish). Then, 10 mm diameter, 10 mm thick NdFeB permanent magnets were placed under the confocal dishes. After incubating at room temperature for 15 min, the cells were washed three times with PBS; the second step was to add 20 μL of 1 mg/mL Andy Fluor 488 labeled streptavidin solution to the confocal center and incubate at room temperature for 15 min; then discard the medium and wash the cells twice with complete medium; in the third step, after dilution with complete culture medium, lipid nanosystem modified with biotin and marked with Did (equivalent to 0.25 μg/mL Did) was added and incubated at 37 °C for 1.5 h. The medium was discarded and the cells were washed twice with culture medium. Finally, the cells were fixed with 4% paraformaldehyde for 10 min at room temperature. Cell nuclei were stained with Hoechst 33,258 and all dishes were scanned using Spinning disk confocal microscope (Ultra VIEW® VoX Spinning Disk, PerkinElmer, Boston, MA, USA). The scanned confocal micrographs were stitched together. For the cell nuclei, the excitation wavelength was 405 nm and the emission wavelength were 445 nm. For the Andy Fluor 488, the excitation wavelength was 488 nm and the emission wavelength was 525 nm. For the Andy Fluor 488, the excitation wavelength was 488 nm and the emission wavelength was 525 nm. For the rhodamine, the excitation wavelength was 561 nm and the emission wavelength was 615 nm. For the Did, the excitation wavelength was 640 nm and the emission wavelength was 705 nm.

2.5. In vivo assay

2.5.1. Infrared image and temperature determination of tumor tissue

Six nude mice bearing A549 tumor (tumor size approximately 500 mm^3) were anesthetized by intraperitoneal injection with 4% chloral hydrate (0.1 mL/10 g). After the nude mice were completely anesthetized, the tumor sites of nude mice were observed with an infrared camera (FOTRIC226, IRS SYSTEMS Inc., Shanghai, China). The results are shown in Supporting Information Table S5. The animal assays were approved by the Ethics Committee of Peking University, Beijing, China.

The nude mice bearing A549 tumors were examined by Multispectral Optoacoustic Tomography (MSOT, 256-channel real-time imaging MSOT scanner, iThera Medical GmbH, Munich, Germany) to observe the distribution of hemoglobin (Hb) and oxyhemoglobin (HbO_2) at the tumor site. Subsequently, the tumor sites were heated to 42−43 °C with an 808 nm laser (MW-GX-808/1−5000 MW, Changchun Laser Optoelectronics Technology Co., Ltd., Changchun, China) and maintained for 10 min. The distribution of Hb and HbO_2 in the tumor sites were recorded by MSOT immediately, 5 and 24 h after laser-heating, respectively.

Figure 2 Cellular uptake by A549 cells with three-step administration without external magnetic field. (A) Schematic illustration of three-step administration. (B) Confocal microscope images of A549 cells with three-step administration without external magnetic field. Step 1: the USPIONs modified with rhodamine (red) and different ligands. Step 2: the streptavidin modified with Andy Fluor 488 (green). Step 3: the lipid nanosystem modified with Did (purple) and biotin. The nucleus were stained with Hoechst 33258 (blue). Group I: the USPIONs modified with c(RGDfK), biotin and rhodamine in step 1, normal steps 2 and 3. Group II: the integrin receptor monoclonal antibodies and the USPIONs modified with c(RGDfK), biotin and rhodamine in step 1, normal steps 2 and 3. Group III: the USPIONs modified with biotin and rhodamine in step 1, normal steps 2 and 3. Group IV: the USPIONs modified with c(RADfK), biotin and rhodamine in step 1, normal steps 2 and 3. Group V: no step 1, normal steps 2 and 3. Group VI: no step 1 and 2, normal step 3. Scale bar: 10 μm. (C) Semi-quantitative analysis of the fluorescence intensities of steps 1−3 in A549 cells which are calculated using gray values. The values are expressed by means ± SD ($n = 30$). ***$P < 0.01$.

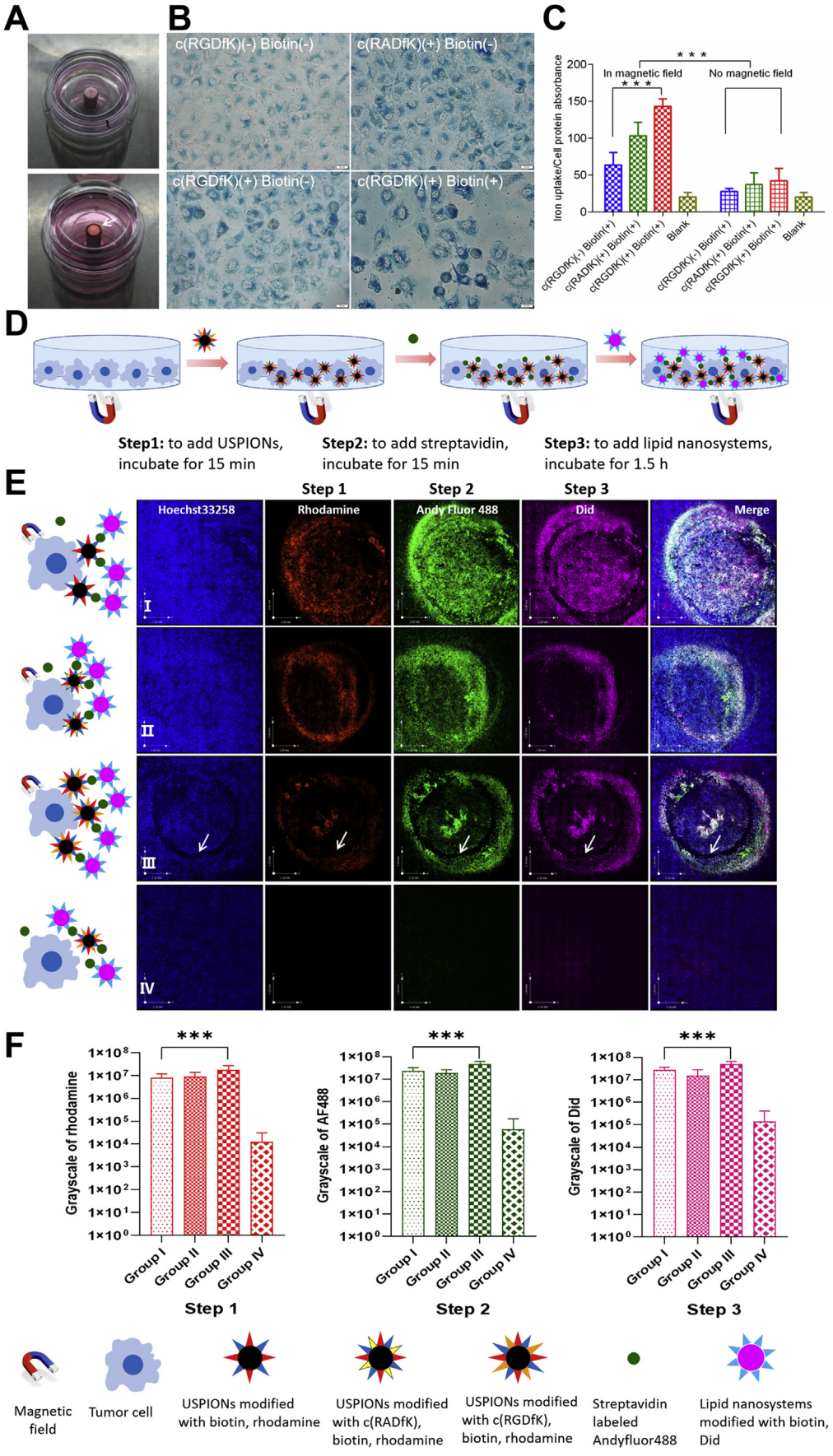
A
B
c(RGDfK)(-) Biotin(-)
c(RADfK)(+) Biotin(-)
c(RGDfK)(+) Biotin(-)
c(RGDfK)(+) Biotin(+)
C
Iron uptake/Cell protein absorbance
In magnetic field
No magnetic field
c(RGDfK)(-) Biotin(+)
c(RADfK)(+) Biotin(+)
c(RGDfK)(+) Biotin(+)
Blank
D
Step1: to add USPIONs, incubate for 15 min
Step2: to add streptavidin, incubate for 15 min
Step3: to add lipid nanosystems, incubate for 1.5 h
E
Step 1
Step 2
Step 3
Hoechst33258
Rhodamine
Andy Fluor 488
Did
Merge
I
II
III
IV
F
Grayscale of rhodamine
Grayscale of AF488
Grayscale of Did
Group I
Group II
Group III
Group IV
Step 1
Step 2
Step 3
Magnetic field
Tumor cell
USPIONs modified with biotin, rhodamine
USPIONs modified with c(RADfK), biotin, rhodamine
USPIONs modified with c(RGDfK), biotin, rhodamine
Streptavidin labeled Andyfluor488
Lipid nanosystems modified with biotin, Did

2.5.2. *In vivo distribution of combination system during three-step delivery*

The nude mice bearing A549 tumor (tumor size approximately 500 mm^3) were randomly divided into six groups, each of which is shown in Supporting Information Table S6.

Experiment procedure had four steps: laser-heating step: the tumor sites were heated to 42−43 °C with 808 nm infrared laser and maintained for 10 min, or without laser-heating; the first step of three-step strategy: USIONPs (modified with c(RGDfK) and biotin, equivalent to 100 μg Fe) labeled with Did were injected into the tail vein, and the tumor sites were put with the external magnetic field (Φ 10 mm × 10 mm NdFeB permanent magnet, 0.55 T, Shanghai Hu Magnetic Industry Co., Ltd., Shanghai, China) for 10 min[29], or without. The second step of three-step strategy: after 3 h, 200 μg streptavidin was injected intraperitoneally into nude mice. The third step of three-step strategy: after 24 h, lipid nanosystem labeled with Dir (equivalent to Dir 0.5 μg) was injected into the tail vein. Did and Dir *in vivo* imaging of tumor-bearing mice was performed 24 h after the third step of administration, and *ex vivo* organ imaging was also performed (CRI Maestro 2, PerkinElmer). For the Did, the excitation wavelength of the first step was 616−661 nm and the emission wavelength was 670−900 nm. For the Dir, the excitation wavelength of the third step was 684−729 nm and the emission wavelength were 740−950 nm.

2.5.3. *In vivo efficacy of magnetism/laser-auxiliary cascaded delivery of combination system*

The efficacy of three-step strategy on tumor growth was assessed by the measurements of tumor volume with an electronic caliper every two days and the observation of tumor weight and size. A549 cells were injected subcutaneously in the back flank of the mice. Forty-nine male nude mice bearing tumor were randomly divided into 7 groups (7 animals in each group) when the tumor reached a volume of 100 mm^3. The data of each group is shown in Supporting Information Table S9.

Experiment procedure had four steps: laser-heating step, the tumor site was treated with 808 nm infrared laser to maintain tumor local temperature at 42−43 °C for 10 min; the first step, USIONPs (modified with c(RGDfK) and biotin, or c(RADfK), equivalent to 100 μg Fe) were injected into the tail vein, and the tumor site was put with the external magnetic field (Φ 10 mm × 10 mm NdFeB permanent magnet, 0.5 T, Shanghai Huci-magnet Co., Ltd., Shanghai, China) for 10 min, or without. The second step, after 3 h, 200 μg streptavidin was injected intraperitoneally into nude mice. The third step, 24 h after the second step, the biotinylated lipid nanosystem containing doxorubicin (equivalent to Dox 4 mg/kg) was injected into the tail vein.

Each chemotherapy group (groups I−VI) received its corresponding treatment on day 1, 8, and 15. The negative control group (group VII) was treated with the same amount of saline. On day 20, the nude mice were sacrificed, and the tumors were taken out for photographs and weighting. During the test, the body weight of mice in each group was also recorded.

3. Results and discussion

3.1. *Preparation of the combination drug system*

Firstly, we tried various approaches including the classical co-precipitation method[30], solvent-thermal method[31,32], microwave method[33,34], polyol method[35−37] and thermal decomposition method[38,39] to synthesize USIONPs. We finally chose the thermal decomposition method ($Fe(acac)_3$ as precursor and oleic acid as stabilizer). The TEM and magnetic curve of USIONPs are shown in Supporting Information Fig. S1.

The USIONPs as a type of non-polar nanoparticles could only be dispersed in non-polar solvents such as *n*-hexane. In order to disperse USPIONs into water and to modify with c(RGDfK) and biotin, we used DSPE-PEG2K-c(RGDfK) and DSPE-PEG2K-biotin as amphiphilic materials to encapsulate the non-polar USPIONs[40] by a phase-transfer method. As a result, the hydrophobic and functional USIONPs could be well dispersed in water. Similarly, the USPIONS could also be modified with biotin, control peptide c(RADfK), rhodamine, Did or Dir. The synthesis routes of DSPE-PEG2K-c(RGDfK) and DSPE-PEG2K-Rhodamine, and the MALDI-TOF-MS of DSPE-PEG2K-Rhodamine, DSPE-PEG2K-c(RGDfK) and DSPE-PEG2K-c(RADfK) are shown in Supporting Information Fig. S2.

3.2. *Characterizations of the combination system*

As shown in Fig. 1A, the morphology of USIONPs modified with c(RGDfK) and biotin as well as their "core−shell" structure could be clearly observed under TEM[41]. The diameter of their FeO core evaluated by TEM was approximately 14 nm. The mean Z-average size of the functional USIONPs determined by dynamic laser light scattering (DLS) was 42.20 nm with a PDI of 0.285, while their zeta potential was −20.8 mV (Fig. 1D). Additionally, the magnetization curve showed that the saturation magnetization of the modified USIONPs was 55 em/g at room temperature, exhibiting superparamagnetic properties (Fig. 1B). Finally,

Figure 3 Cellular uptake by A549 cells with external magnetic field. (A) Distribution of USPIONs in confocal dishes under external magnetic field conditions. White arrows indicate USPIONS aggregation. (B) Prussian blue-stained A549 cells incubated with USPIONs modified without c(RGDfK) and biotin as the blank control, USPIONs modified with c(RADfK) and without biotin, USPIONs modified with c(RGDfK) and without biotin, as well as USPIONs modified with c(RGDfK) and biotin. The USPIONs was detected with the Prussian blue histological staining (blue). Scale bar: 20 μm. (C) Quantitative analysis of USPIONs cellular uptake in A549 cells is calculated using iron absorption and protein ratio by ICP-MS. Values expressed are means±S.D. ($n=4$). ***$P < 0.01$ *vs*. control. (D) Schematic illustration of three-step administration. (E) Confocal microscope images of A549 cells with three-step administration and external magnetic field. Step 1: the USPIONs modified with the rhodamine (red) and different ligand. Step 2: the streptavidin modified with Andy Fluor488 (green). Step 3: the lipid nanosystems modified with Did (purple) and biotin. The nucleus was stained with Hoechst33258 (blue). Group I: the USPIONs modified with biotin and rhodamine in step 1, normal steps 2 and 3, with external magnetic field. Group II: the USPIONs modified with c(RADfK), biotin and rhodamine in step 1, normal steps 2 and 3, with external magnetic field. Group III: the USPIONs modified with c(RGDfK), biotin and rhodamine in step 1, normal steps 2 and 3, with external magnetic field. Group IV: the USPIONs modified with c(RGDfK), biotin and rhodamine in step 1, normal steps 2 and 3, but without external magnetic field. Scale bar: 1 mm. (F) Semi-quantitative analysis of the fluorescence intensities of steps 1−3 in different areas which are calculated using gray values. The values are expressed by means±S.D. ($n=9$). ***$P<0.01$.

MALDI-TOF of the functional USPIONs confirmed the conjugation of both c(RGDfK) and biotin (Fig. 1C).

The thin film dispersion method[42] was utilized to prepare lipid nanosystem modified with biotin by adding DSPE-PEG2K-biotin during the fabrication. The modified nanosystems were loaded with doxorubicin by ammonium sulfate gradient method. The particle size of final nanosystems determined by DLS was 94.7 nm with a PDI of 0.180, and their zeta potential was −10.6 mV (Fig. 1E).

3.3. Cellular uptake assay

3.3.1. Endocytosis of combination system via three-step delivery without external magnetic field

In the absence of a magnetic field, cellular uptake of combination system *via* three-step strategy was then investigated (Table S1 and Fig. 2). The procedure of three-step administration is illustrated in Fig. 2A, the confocal images of A549 cells with three-step administration are shown in Fig. 2B, and the fluorescence intensities of each step are summarized in Fig. 2C and Supporting Information Table S2. Generally, the strongest signals were found in each step of group I, followed by groups IV, III and II. Groups V and VI showed almost no signals.

As seen in group I, the modifications with both c(RGDfK) and biotin had the strongest effect in terms of enhancing cell uptake of USPIONs in step 1, leading to the strongest binding of streptavidin in step 2 as well as that of biotin-modified lipid nanosystem in step 3. The obvious intracellular distribution of signals was likely owing to the integrin-c(RGDfK) mediated endocytosis. The three kinds of fluorescence well co-localized with each other, indicating the exact delivery process step by step as we designed.

After blocking the integrin with monoantibody as shown in group II, the fluorescence in first step attenuated obviously, so there might be little USPIONs on the cells. Since little biotin was available due to the lack of nanoparticles on the cells, the second signal by labeled streptavidin was also weak.

The use of USPIONs with biotin but without c(RGDfK) in the step 1 of group III led to weaker fluorescence mainly on the cell surface in all three steps, compared to group I. The obvious signals specially in step 2 revealed some degree of interaction between biotin and cell surface in step 1, which caused weaker but obvious association at the following steps 2 and 3. In addition, the difference between groups I and III reflected the key role of RGD in term of more cell internalization.

In the first step of group IV, the normal peptide was replaced by a disorder peptide, which triggered an obvious fluorescence in steps 1 to 3, slightly stronger than group III but weaker than group I, with partial intracellular signals. The difference between groups IV and I confirmed the stronger effect of RGD peptide than random peptide. The comparison between groups IV and III demonstrated the effect of disorder peptide, which resulted in more cell internalization and explained the stronger fluorescence than that in group III in all steps.

As illustrated in group V, without the first step delivery of nanoparticles, there was basically no invisible fluorescence at steps 2 and 3, indicating the importance of the first delivery, namely streptavidin could not interact directly with the cells. In group VI, the lack of first and second step delivery caused no any fluorescence in the third step, suggesting that the interaction between lipid nanosystems and cells in step 3 was weak. Generally, this study demonstrated here that such a three-step approach might be a potential delivery strategy, at least *in vitro*.

3.3.2. Cellular uptake of USIONPs with external magnetic field

We tried to use an NdFeB permanent magnet as external magnetic fields to further enhance the uptake of USPIONs by A549 cells. As shown in Fig. 3, when the magnetic field was placed under the confocal dish, the USPIONs accumulated at the edge of magnetic field to form a circle (Fig. 3A), indicating the efficient impact of external magnetic field to USPIONs in the test condition. By using the Prussian blue method[43] (Fig. 3B), we found that the USPIONs modified with c(RGDfK) and biotin exhibited the highest uptake in A549 in the external magnetic field. While, the cell uptake of USPIONs modified only with c(RGDfK) or c(RADfK) was obvious. The USPIONs modified only with biotin had the least uptake.

Besides the qualitative study, we used the ICP-MS method[34] to further quantify the amount of USPIONs inside of cells. As seen in Fig. 3C, the difference in cell uptake between test groups with and without magnetic field was extremely significant ($P = 1.94 \times 10^{-7}$). Namely, the external magnetic field could enhance the A549 cellular uptake for all types of USPIONs. In the presence of external magnetic field, the order of cellular uptake level of USPIONs was: USPIONs modified with c(RGDfK) and biotin > USPIONs modified with c(RADfK) and biotin > USPIONs only modified with biotin. On the other hand, in the absence of magnetic field there was no significant difference in terms of uptake amount of USPIONs among all test groups ($P = 0.0995$). Generally, the external magnetic field could further promote the cellular uptake of USPIONs based on peptide and biotin conjugation, and especially magnify the distinctions among different test groups.

3.3.3. Endocytosis of combination system via cascaded delivery with external magnetic field

The operation schematic illustration of such an endocytosis study is shown in Fig. 3D, the observations are summarized in Fig. 3E, and fluorescence intensities are recorded in Fig. 3F. *Via* the comparison between group IV and other groups (Table S3), it was clear that the cellular uptake of combination system *via* three-step strategy with magnetic fields was significantly higher than that without magnetic fields. The fluorescence intensity values of step 1 from groups I to IV are shown in Supporting Information Table S4. Generally, the signals in steps 1, 2 and 3 for groups I–III were significant different ($P < 0.01$). The strongest fluorescence was found in each step of group III, the signals between groups I and II in each step seemed similar in intensity, and group IV only had almost no fluorescence. Finally, the fluorescence in each step was well co-localized with each other in groups I, II or III, as seen from the merging images.

This study demonstrated directly that the magnetic fields enhanced significantly the cell uptake of USPIONs. The well co-localization of fluorescence signals in each step indicated the same targeting site for each delivery. Significant difference among groups I, II and III suggested that the combination of c(RGDfK) and external magnetic fields could enhance the cellular uptake of A549 *in vitro*.

3.4. In vivo assay

It will be more complicated *in vivo*, where magnetic field intensity is compromised by distance, tissue, blood flow, and so forth. In

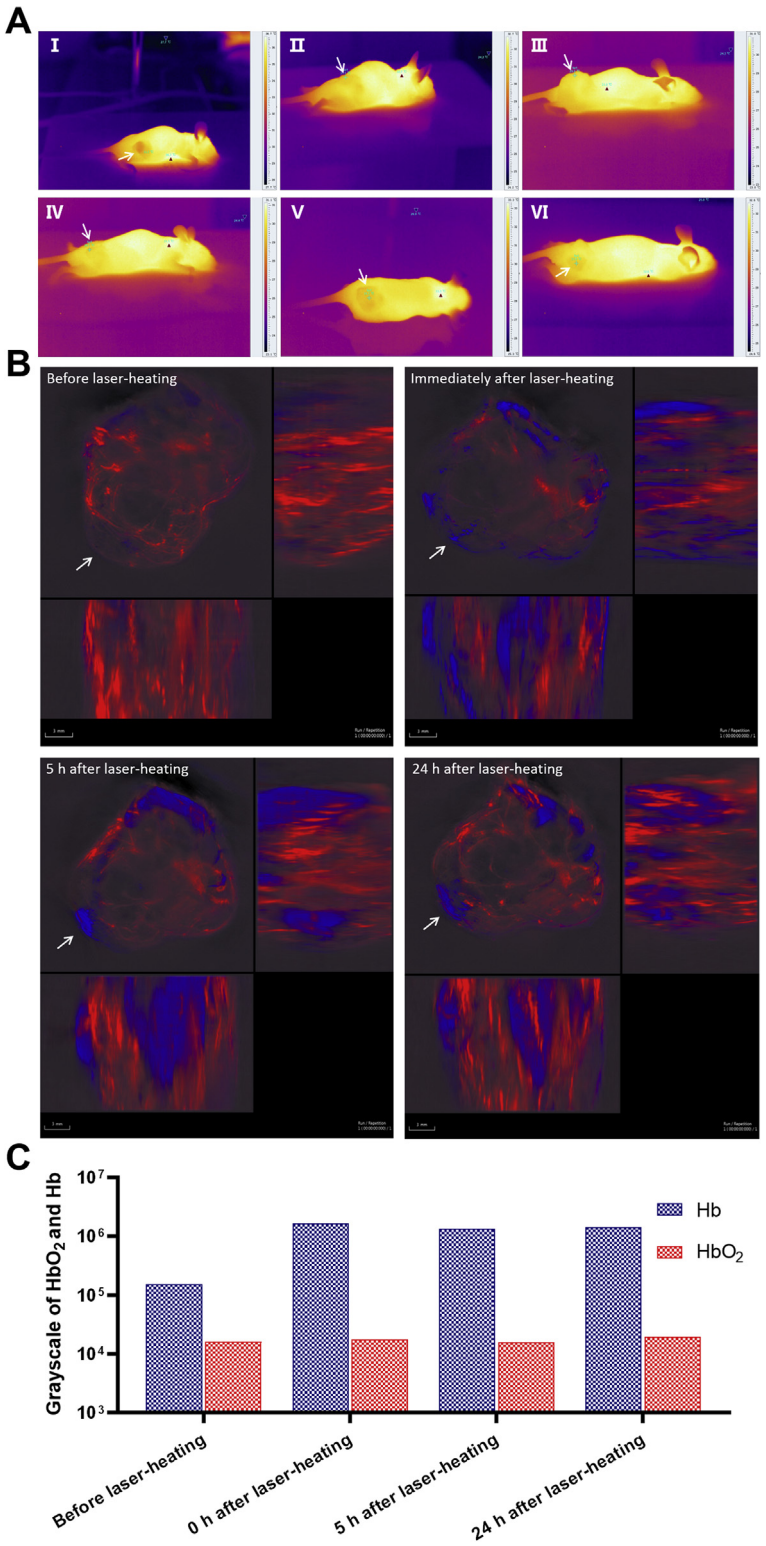

Figure 4 The blood supply in nu/nu mice bearing A549 tumors before and after laser-heating treatment. (A) Infrared images of six tumor-bearing nude mice (form I to VI). The arrow refers to the tumor. The brighter the part, the higher the temperature. (B) Photoacoustic images of tumor site before and after laser-heating, including photoacoustic images of tumor site before laser-heating (top left), photoacoustic images immediately after laser-heating (top right), photoacoustic images 5 h after laser-heating (down left), and photoacoustic images 24 h after laser-heating (down right). The condition of laser-heating is to irradiate the tumor site with a laser having a wavelength of 808 nm, and maintain the temperature of the tumor site at 42−43 °C for 10 min. Each photoacoustic image is divided into three different directions: a merge image of the body parts with tumors from front to back (upper left image), from right to left (upper right image), from bottom to top (lower left image). The arrow points to the tumor site. Red is signal of oxyhemoglobin (HbO_2), which indicates the supply of arterial blood flow. Blue is signal of deoxyhemoglobin (Hb), which indicates venous flow. Scale bar: 3 mm. (C) Semi-quantitative analysis of the signal intensities of Hb and HbO_2 in different stages of laser-heating which are calculated using gray values.

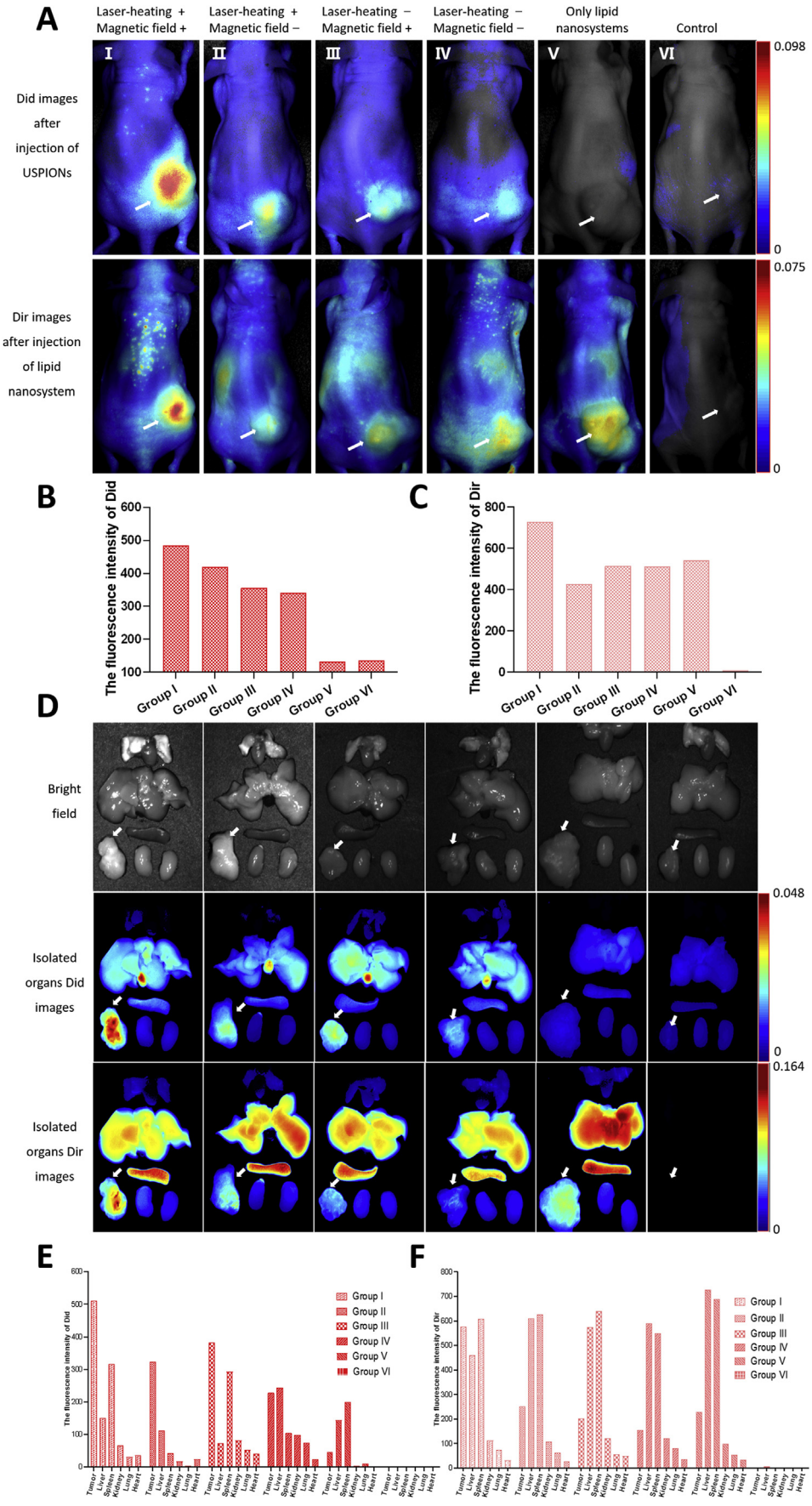
A
Laser-heating + Magnetic field +
Laser-heating + Magnetic field −
Laser-heating − Magnetic field +
Laser-heating − Magnetic field −
Only lipid nanosystems
Control
I
II
III
IV
V
VI
0.098
0
Did images after injection of USPIONs
Dir images after injection of lipid nanosystem
0.075
0
B
The fluorescence intensity of Did
600
500
400
300
200
100
Group I
Group II
Group III
Group IV
Group V
Group VI
C
The fluorescence intensity of Dir
800
600
400
200
0
D
Bright field
Isolated organs Did images
0.048
0
Isolated organs Dir images
0.164
0
E
F
Tumor
Liver
Spleen
Kidney
Lung
Heart

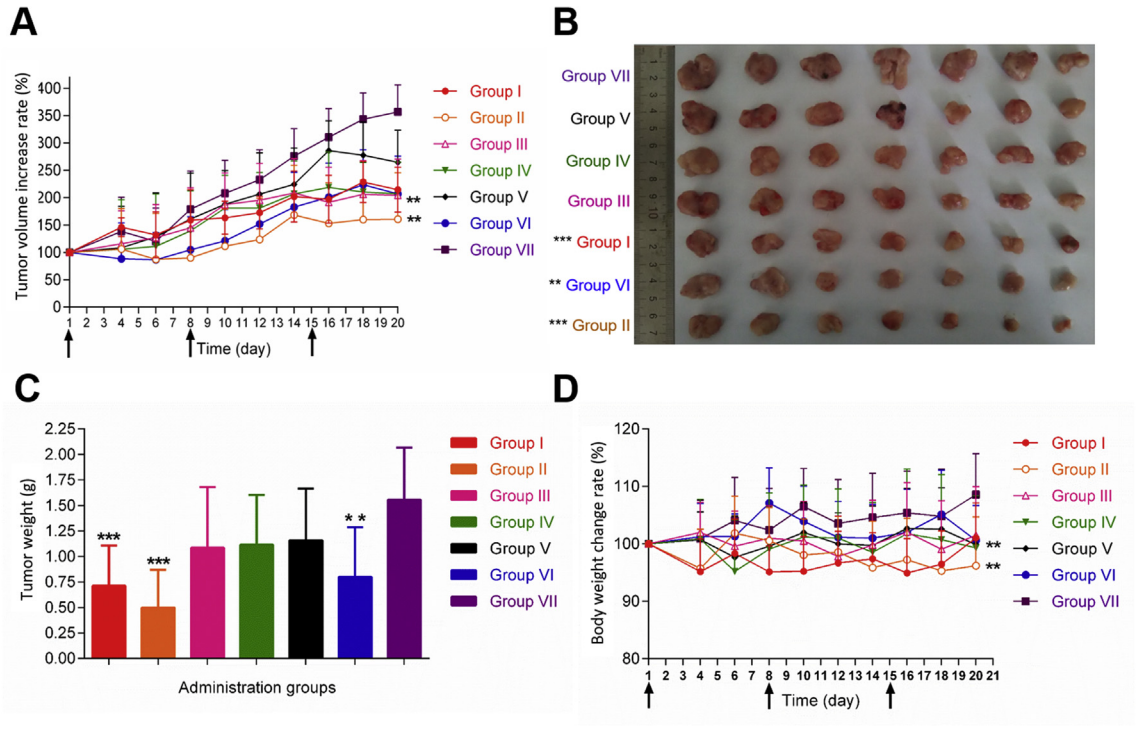

Figure 6 *In vivo* therapeutic efficacy. Group I: with the laser-heating process, without magnetic field, three-step treatment (USPIONs modified with c(RGDfK) and biotin); group II: with the laser-heating process, with magnetic field, three-step treatment (USPIONs modified with c(RGDfK) and biotin); group III: with the laser-heating process, with magnetic field, three-step treatment (USPIONs modified with c(RADfK) and biotin); group IV: without the laser-heating process, with magnetic field, three-step treatment (USPIONs modified with c(RGDfK) and biotin); group V: without the laser-heating process, without magnetic field, three-step treatment (USPIONs modified with c(RGDfK) and biotin); group VI: only lipid nanosystems loaded Dox (positive control); group VII: only saline (negative control). Laser-heating process: the tumor site with 808 nm infrared laser irradiation, to maintain tumor local temperature 42−43 °C 10 min; with magnetic field: the tumor sites with the external magnetic field (Φ 10 mm × 10 mm NdFeB permanent magnet) for 10 min; three-step treatment: the first step: USPIONs (modified with c(RGDfK) and biotin, or c(RADfK), equivalent to 100 μg Fe) were injected into the tail vein; the second step: after 3 h, 200 μg streptavidin was injected intraperitoneally into nude mice; the third step: 24 h after the second step, to inject biotinylated lipid nanosystems containing doxorubicin (equivalent to Dox 4 mg/kg) (A) The tumor growth curve of tumor-bearing mice after treatment for 20 days (B) Photographs of tumors removed from mice 20 days (C) average tumor weight (D) changes in body weight of mice during the 20 days of dosing. Values expressed are means ± SD ($n = 7$). $^{**}P < 0.05$ *vs*. negative control. $^{***}P < 0.01$ *vs*. negative control. The arrows indicate the time of dosing.

other words, the impact of magnetic field on the behave of USPIONs in deep tissue might be very different, so it is essential to conduct animal test to demonstrate the *in vivo* targeting effect of double modified USPIONs.

3.4.1. Infrared image and temperature determination of tumor tissue

Using the infrared camera, we found that the color of tumor area was obviously darker (Fig. 4A), and the temperature in the tumor

Figure 5 The fluorescence images of nu/nu mice bearing A549 tumors after the three step treatments in different conditions. (A) *In vivo* fluorescence images of tumor-bearing nude mice after the three step treatments in different conditions. Laser-heating: the tumor site is irradiated by 808 nm laser, maintaining 42−43 °C for 10 min. Magnetic field: place NdFeB permanent magnets on the tumor site for 10 min. Group I: after laser-heating, intravenous injection of Did labelled USPIONs modified with c(RGDfK) and biotin (equivalent to 100 μg Fe) was conducted, followed by placing in a magnetic field at the tumor site for 10 min. Three hours after injection of USPIONs, 200 μg streptavidin was given by intraperitoneal injection. Twenty-four hours after injection of streptavidin, *in vivo* Did fluorescence imaging of mice was recorded, as shown in the first row of Fig. 5A, and then intravenous injection of Dir labelled lipid nanosystems was given. Twenty-four hours after injection of lipid nanosystems, the *in vivo* Dir fluorescence imaging of mice was recorded, as shown in the second row of Fig. 5A. Group II: no magnetic field, others are the same as the group I. Group III: no laser-heating, others are the same as the group I. Group IV: no magnetic field and laser-heating, others are the same as the group I. Group V: only intravenous injection of Dir labeled lipid nanosystems modified with biotin. Group VI: intravenous injection of saline as the control. (B) Semi-quantitative analysis of the fluorescence intensities of Did and. (C) Dir *in vivo*. (D) *Ex vivo* bright field images of major organs and tumors 24 h after the last injection of three steps (the first row). *Ex vivo* Did fluorescence images of major organs and tumors 24 h after the second injection of three steps (the second row). *Ex vivo* Did fluorescence images of major organs and tumors 24 h after the last injection of three steps (the third row). From the top to the bottom, the isolated organs are lung, heart, liver, spleen and kidney. The arrow refers to the tumor. (E) Semi-quantitative analysis of the fluorescence intensities of Did and (F) Dir in the isolated organ tissues.

site was 1−3 °C lower than normal tissue (Table S5), suggesting that the blood supply to the A549 tumor tissue might be less than normal site.

Photoacoustic imaging was recorded to further study the blood supply to the A549 tumor tissue. As shown in Fig. 4B, red was the signal of oxyhemoglobin (HbO_2), which indicated the supply of arterial blood flow. While, blue was the signal of hemoglobin (Hb), which indicated the venous flow. The signal intensities of Hb and HbO_2 in different stages of laser-heating was then calculated (Fig. 4C). Briefly, the blue signal of Hb was always higher than the red one of HbO_2 in all test time points. The signal of HbO_2 kept unchanged before and after laser treatment, while that of Hb showed obvious alteration after laser-heating. From 0 to 24 h post treatment, basically there were no signal changes for both Hb and HbO_2. The results clearly revealed that the laser-heating process was efficient in terms of promoting the permeability of tumor venous blood vessels and enhancing the venous flow, which could maintain up to 24 h. The increase in permeability of tumor venous blood vessels might mean the improvement of EPR effect.

3.4.2. *In vivo distribution of combination system during three-step delivery*

In order to further evaluate the targeting efficiency for the three-step delivery of the combination system, we performed near-infrared fluorescence imaging in A549 bearing nude mice (Figs. S3 and 5A, Table S6), and the fluorescence intensity of the tumor site was also recorded (Fig. 5B and C).

As shown in Fig. 5A−C, the signal of Did indicating USPIONs and Dir indicating lipid nanosystems in all groups with three-step delivery was obviously stronger than that of saline control. Especially, the cascaded delivery together with laser-heating and magnetic fields (group I) achieved the highest distribution in tumor, as seen by the strongest signals of both Did and Dir. Additionally, the fluorescence intensity of Did was very low and that of Dir was relatively high in group V because no functional USPIONs but only lipid nanosystems were given in this group. For other groups, the signals were basically consistent in tendency between Did and Dir groups, revealing the connection between the steps 1 and 3. It was worthwhile to mention however, that the image analysis of living animal had limitations, and it only provided general or rough information, due to the complicated *in vivo* situation. For instance, we did not find the clear evidence that laser-heating improved the targeting effects of modified USPIONs, but external magnetic field somehow enhanced the Did signals of nanoparticles in tumor.

Ex vivo images of dissected tumors and main organ tissues are illustrated in Fig. 5D, and the fluorescence intensities of the isolated tumors are shown in Fig. 5E and F (Supporting Information Tables S7 and S8). The fluorescence signals of Did and Dir in tumors were basically similar with above observations. Interestingly, the *ex vivo* study provided more clearer images in terms of fluorescence distribution in tissues, which was favorable for the comparison between cancer and tissues. Based on the Did signal, the double modified USPIONs accumulated more in liver, but less in other organs. Besides, the functional USPIONs in tumor was obviously higher in group I than those in groups II−IV.

Based on the Dir signal, it was found that lipid nanosystem distributed more in liver and spleen, but less in lung and kidney, with group V as the typical example. Again, in group I, the lipid nanosystems in tumor was clearly higher than those in groups II−IV. Additionally, in groups II−V, the lipid nanosystem distribution in tumor was obvious less than those in liver and spleen. However, only in group I, the lipid nanosystem accumulation in tumor site was evidently more than that in liver.

Based on the observation on group IV, it seemed that the double modified USPIONs themselves demonstrated limited targeting *in vivo*, which led to limited tumor accumulation of lipid nanosystem, as Did and Dir signals indicated. It was different from the fact of cell test, in which nanoparticles could readily contact with cells. So, the complicated situation *in vivo* compromised the targeting efficacy and it is necessary to use other means to promote the delivery. With only laser-heating or external magnetic field, the targeting effects of double modified USPIONs improved, but still with more accumulation in liver or kidney compared to tumor. Only the combination of three-step delivery with laser-heating and magnetic fields realized high tumor distribution than all other tissues. Finally, the first step of three step strategy was fatal in guaranteeing the efficient delivery. Generally, this study demonstrated the necessity of combining physical, biological and chemical means of targeting, although it did not provide evidence for intracellular drug storage which might more closely relate to antitumor efficacy.

3.4.3. *In vivo efficacy of magnetism/laser-auxiliary cascaded delivery of combination system*

Fig. 6A illustrates the tumor growth curve of tumor-bearing mice after different treatments (Table S9). It was found that in the presence of laser and magnetic field, the USPIONs modified with c(RGDfK) and biotin showed the best antitumor efficacy among all treatments. The weight of isolated tumor as shown in Fig. 6B and C confirmed the same conclusion. The body weight loss of nude mice in groups II and VI was different from that in negative control (Fig. 6D). The comparison between groups II and IV revealed the significance of laser treatment, because the three-step delivery without laser (group IV) was no difference from the negative control. Similarly, the comparison between groups II and I demonstrated the importance of magnetic field further, since the multiple deliveries with magnetic field resulted in less tumor volume and weight. Based on the comparison between groups II and III, it seemed that c(RGDfK) conjugation was also essential, as the targeted delivery with c(RADfK) made no difference from the negative control. Finally, the comparison between groups I and IV indicated the stronger impact of laser-heating than magnetic fields, but without significance. In short, the combination of all these approaches achieved the most inhibition on tumor. By the way, there might be further room for improvement in terms of increasing magnetic field strength, optimizing the intensity of laser-heating and screening better regimen of three-step strategy.

4. Conclusions

In summary, there are a huge numbers of investigations on targeted drug delivery[44−47], but their clinic translational process seems not very smooth,[48,49], which should cause our high attention. Given the complexity of the human body and tumors, a single delivery strategy is generally inefficient[50], while a fancy delivery system seems very impractical[50−54]. Based on some well-confirmed delivery approaches, it might be possible to greatly improve the targeting efficiency by making use of different targeting principles and their coordination to the best of our ability.

Here, we design and investigate the tumor therapy *via* a magnetism/laser-auxiliary three-step delivery of a combination

system for the proof-of-concept. It is expected that the blood supply in the tumor site will be improved firstly by the irradiation with a laser treatment. In the presence of a magnetic field, the USPIONs modified with c(RGDfK) and biotin could target to the tumor site by both magnetism and chemical association of RGD-integrin. Subsequently, the injected streptavidin will specifically deliver to USPIONs by avidin−biotin binding. Finally, Dox nanosystems modified with biotin will transport to streptavidin already there by the biological effect.

Fortunately, the *in vitro* and *in vivo* study demonstrated a positive conclusion here. *In vitro*, the specificity of c(RGDfK), the merit of cascaded strategy and the impact of external magnetic field, were demonstrated in A549 cells. *In vivo*, it was found that the magnetism/laser-auxiliary cascaded delivery of such a combination system showed the strongest targeting delivery to tumor tissue, as well as the best antitumor efficacy. This study demonstrates the necessity of such a combination of physical, chemical and biological targeting and provides a new insight into the nanotechnology-based targeted anticancer therapy.

Acknowledgments

This work is financially supported by the National Basic Research Program of China (2015CB932100), the National Natural Science Foundation of China (81690264 and 81821004), and the Foundation for the Innovation Team of Ministry of Education (No. BMU2017TD003, China).

Author contributions

Qiang Zhang provided ideas, conceived and designed experiments, amended the manuscript; Jialiang Lin perfected ideas, carried out experiments, analyzed experimental data and results, wrote the manuscript; Qingqing Yin assisted with carrying out experiments; Binlong Chen, Haoran Zhang, Dong Mei, and Jijun Fu assisted with analyzing experimental data; Bing He, Hua Zhang, Wenbing Dai, Xueqing Wang, and Yiguang Wang assisted with amending the manuscript.

Conflicts of interest

The authors declare that there are no conflicts of interest.

Appendix A. Supporting information

Supporting data to this article can be found online at https://doi.org/10.1016/j.apsb.2019.12.017.

References

1. Li C, Wang J, Wang Y, Gao H, Wei G, Huang Y, et al. Recent progress in drug delivery. *Acta Pharm Sin B* 2019;**9**:1145−62.
2. Yang Y, Chen S, Li H, Yuan Y, Zhang Z, Xie J, et al. Engineered paramagnetic graphene quantum dots with enhanced relaxivity for tumor imaging. *Nano Lett* 2018;**19**:441−8.
3. He S, Fan W, Wu N, Zhu J, Miao Y, Miao X, et al. Lipid-based liquid crystalline nanoparticles facilitate cytosolic delivery of siRNA *via* structural transformation. *Nano Lett* 2018;**18**:2411−9.
4. Shi J, Kantoff PW, Wooster R, Farokhzad OC. Cancer nanomedicine: progress, challenges and opportunities. *Nat Rev Cancer* 2017;**17**:20−37.
5. Hassan S, Prakash G, Ozturk A, Saghazadeh S, Sohail MF, Seo J, et al. Evolution and clinical translation of drug delivery nanomaterials. *Nano Today* 2017;**15**:91−106.
6. Chen H, Zhang W, Zhu G, Xie J, Chen X. Rethinking cancer nanotheranostics. *Nat Rev Mater* 2017;**2**:17024.
7. Lazarovits J, Chen YY, Sykes EA, Chan WC. Nanoparticle-blood interactions: the implications on solid tumour targeting. *Chem Commun* 2015;**51**:2756−67.
8. Bertrand N, Grenier P, Mahmoudi M, Lima EM, Appel EA, Dormont F, et al. Mechanistic understanding of *in vivo* protein corona formation on polymeric nanoparticles and impact on pharmacokinetics. *Nat Commun* 2017;**8**:777.
9. Lammers T, Kiessling F, Ashford M, Hennink W, Crommelin D, Storm G. Cancer nanomedicine: is targeting our target?. *Nat Rev Mater* 2016;**1**:16069.
10. Dai Y, Xu C, Sun X, Chen X. Nanoparticle design strategies for enhanced anticancer therapy by exploiting the tumour microenvironment. *Chem Soc Rev* 2017;**46**:3830−52.
11. Matsumoto Y, Nichols JW, Toh K, Nomoto T, Cabral H, Miura Y, et al. Vascular bursts enhance permeability of tumour blood vessels and improve nanoparticle delivery. *Nat Nanotechnol* 2016;**11**:533−8.
12. He Y, Shirazaki M, Liu H, Himeno R, Sun Z. A numerical coupling model to analyze the blood flow, temperature, and oxygen transport in human breast tumor under laser irradiation. *Comput Biol Med* 2006;**36**:1336−50.
13. Sen A, Capitano ML, Spernyak JA, Schueckler JT, Thomas S, Singh AK, et al. Mild elevation of body temperature reduces tumor interstitial fluid pressure and hypoxia and enhances efficacy of radiotherapy in murine tumor models. *Cancer Res* 2011;**71**:3872−80.
14. Sun T, Zhang G, Wang Q, Chen Q, Chen X, Lu Y, et al. A targeting theranostics nanomedicine as an alternative approach for hyperthermia perfusion. *Biomaterials* 2018;**183**:268−79.
15. Singh S, Siriwardana PN, Johnston EW, Watkins J, Bandula S, Illing R, et al. Perivascular extension of microwave ablation zone: demonstrated using an *ex vivo* porcine perfusion liver model. *Int J Hyperth* 2018;**34**:1114−20.
16. Zhang L, Zhu H, Jin C, Zhou K, Li K, Su H, et al. High-intensity focused ultrasound (HIFU): effective and safe therapy for hepatocellular carcinoma adjacent to major hepatic veins. *Eur Radiol* 2009;**19**:437−45.
17. Song X, Li R, Deng H, Li Y, Cui Y, Zhang H, et al. Receptor mediated transcytosis in biological barrier: the influence of receptor character and their ligand density on the transmembrane pathway of active-targeting nanocarriers. *Biomaterials* 2018;**180**:78−90.
18. Wang D, Fu J, Shi Y, Peng D, Yuan L, He B, et al. The modulation of tumor vessel permeability by thalidomide and its impacts on different types of targeted drug delivery systems in a sarcoma mouse model. *J Control Release* 2016;**238**:186−96.
19. Wang P, Zhang L, Zheng W, Cong L, Guo Z, Xie Y, et al. Thermo-triggered release of CRISPR-Cas9 system by lipid-encapsulated gold nanoparticles for tumor therapy. *Angew Chem Int Ed Engl* 2018;**57**:1491−6.
20. Ma K, Fu D, Yu D, Cui C, Wang L, Guo Z, et al. Targeted delivery of *in situ* PCR-amplified sleeping beauty transposon genes to cancer cells with lipid-based nanoparticle-like protocells. *Biomaterials* 2017;**121**:55−63.
21. Chee HL, Gan CRR, Ng M, Low L, Fernig DG, Bhakoo KK, et al. Biocompatible peptide-coated ultrasmall superparamagnetic iron oxide nanoparticles for *in vivo* contrast-enhanced magnetic resonance imaging. *ACS Nano* 2018;**12**:6480−91.
22. Chilkoti A, Tan PH, Stayton PS. Site-directed mutagenesis studies of the high-affinity streptavidin−biotin complex: contributions of tryptophan residues 79, 108, and 120. *Proc Natl Acad Sci U S A* 1995;**92**:1754−8.
23. Liu W, Samanta SK, Smith BD, Isaacs L. Synthetic mimics of biotin/(strept)avidin. *Chem Soc Rev* 2017;**46**:2391−403.
24. Patra M, Zarschler K, Pietzsch HJ, Stephan H, Gasser G. New insights into the pretargeting approach to image and treat tumours. *Chem Soc Rev* 2016;**45**:6415−31.

25. Wu YP, Chew CY, Li TN, Chung TH, Chang EH, Lam CH, et al. Target-activated streptavidin-biotin controlled binding probe. *Chem Sci* 2018;**9**:770−6.
26. Sreekanth KV, Alapan Y, ElKabbash M, Ilker E, Hinczewski M, Gurkan UA, et al. Extreme sensitivity biosensing platform based on hyperbolic metamaterials. *Nat Mater* 2016;**15**:621−7.
27. Sugahara KN, Teesalu T, Karmali PP, Kotamraju VR, Agemy L, Girard OM, et al. Tissue-penetrating delivery of compounds and nanoparticles into tumors. *Cancer Cell* 2009;**16**:510−20.
28. Siegel RL, Miller KD, Jemal A. Cancer statistics. *CA Cancer J Clin* 2019;**69**:7−34.
29. Mejias R, Perez-Yague S, Gutierrez L, Cabrera LI, Spada R, Acedo P, et al. Dimercaptosuccinic acid-coated magnetite nanoparticles for magnetically guided *in vivo* delivery of interferon gamma for cancer immunotherapy. *Biomaterials* 2011;**32**:2938−52.
30. Massart R. Preparation of aqueous magnetic liquids in alkaline and acidic media. *Ieee T Magn* 1981;**17**:1247−8.
31. Pinna N, Grancharov S, Beato P, Bonville P, Antonietti M, Niederberger M. Magnetite nanocrystals: nonaqueous synthesis, characterization, and solubility. *Chem Mater* 2005;**17**:3044−9.
32. Liu J, Sun Z, Deng Y, Zou Y, Li C, Guo X, et al. Highly water-dispersible biocompatible magnetite particles with low cytotoxicity stabilized by citrate groups. *Angew Chem Int Ed Engl* 2009;**48**:5875−9.
33. Yang Y, Guo Q, Peng J, Su J, Lu X, Zhao Y, et al. Doxorubicin-conjugated heparin-coated superparamagnetic iron oxide nanoparticles for combined anticancer drug delivery and magnetic resonance imaging. *J Biomed Nanotechnol* 2016;**12**:1963−74.
34. Carenza E, Barcelo V, Morancho A, Montaner J, Rosell A, Roig A. Rapid synthesis of water-dispersible superparamagnetic iron oxide nanoparticles by a microwave-assisted route for safe labeling of endothelial progenitor cells. *Acta Biomater* 2014;**10**:3775−85.
35. Ge J, Hu Y, Biasini M, Beyermann WP, Yin Y. Superparamagnetic magnetite colloidal nanocrystal clusters. *Angew Chem Int Ed Engl* 2007;**46**:4342−5.
36. Deng H, Li X, Peng Q, Wang X, Chen J, Li Y. Monodisperse magnetic single-crystal ferrite microspheres. *Angew Chem Int Ed Engl* 2005;**44**:2782−5.
37. Xue S, Zhang C, Yang Y, Zhang L, Cheng D, Zhang J, et al. 99mTc-Labeled iron oxide nanoparticles for dual-contrast (T_1/T_2) magnetic resonance and dual-modality imaging of tumor angiogenesis. *J Biomed Nanotechnol* 2015;**11**:1027−37.
38. Hou Y, Xu Z, Sun S. Controlled synthesis and chemical conversions of FeO nanoparticles. *Angew Chem Int Ed Engl* 2007;**46**:4342−5.
39. Yu WW, Falkner JC, Yavuz CT, Colvin VL. Synthesis of monodisperse iron oxide nanocrystals by thermal decomposition of iron carboxylate salts. *Chem Commun* 2004:2306−7.
40. Hao R, Yu J, Ge Z, Zhao L, Sheng F, Xu L, et al. Developing Fe_3O_4 nanoparticles into an efficient multimodality imaging and therapeutic probe. *Nanoscale* 2013;**5**:11954−63.
41. Ruiz-de-Angulo A, Zabaleta A, Gomez-Vallejo V, Llop J, Mareque-Rivas JC. Microdosed lipid-coated ^{67}Ga-magnetite enhances antigen-specific immunity by image tracked delivery of antigen and CpG to lymph nodes. *ACS Nano* 2016;**10**:1602−18.
42. Khemtong C, Togao O, Ren J, Kessinger CW, Takahashi M, Sherry AD, et al. Off-resonance saturation MRI of superparamagnetic nanoprobes: theoretical models and experimental validations. *J Magn Reson* 2011;**209**:53−60.
43. Guo Z, He B, Jin H, Zhang H, Dai W, Zhang L, et al. Targeting efficiency of RGD-modified nanocarriers with different ligand intervals in response to integrin $\alpha v\beta 3$ clustering. *Biomaterials* 2014;**35**:6106−17.
44. Zheng SW, Huang M, Hong RY, Deng SM, Cheng LF, Gao B, et al. RGD-conjugated iron oxide magnetic nanoparticles for magnetic resonance imaging contrast enhancement and hyperthermia. *J Biomater Appl* 2014;**28**:1051−9.
45. Wen J, Yang K, Liu F, Li H, Xu Y, Sun S. Diverse gatekeepers for mesoporous silica nanoparticle based drug delivery systems. *Chem Soc Rev* 2017;**46**:6024−45.
46. Ulbrich K, Hola K, Subr V, Bakandritsos A, Tucek J, Zboril R. Targeted drug delivery with polymers and magnetic nanoparticles: covalent and noncovalent approaches, release control, and clinical studies. *Chem Rev* 2016;**116**:5338−431.
47. Cully M. Drug delivery: nanoparticles improve profile of molecularly targeted cancer drug. *Nat Rev Drug Discov* 2016;**15**:231.
48. Bobo D, Robinson KJ, Islam J, Thurecht KJ, Corrie SR. Nanoparticle-based medicines: a review of FDA-approved materials and clinical trials to date. *Pharm Res* 2016;**33**:2373−87.
49. Ragelle H, Danhier F, Preat V, Langer R, Anderson DG. Nanoparticle-based drug delivery systems: a commercial and regulatory outlook as the field matures. *Expert Opin Drug Deliv* 2017;**14**:851−64.
50. Fan W, Yung B, Huang P, Chen X. Nanotechnology for multimodal synergistic cancer therapy. *Chem Rev* 2017;**117**:13566−638.
51. Song X, Xu J, Liang C, Chao Y, Jin Q, Wang C, et al. Self-supplied tumor oxygenation through separated Liposomal delivery of H_2O_2 and catalase for enhanced radio-immunotherapy of cancer. *Nano Lett* 2018;**18**:6360−8.
52. Yang G, Xu L, Chao Y, Xu J, Sun X, Wu Y, et al. Hollow MnO_2 as a tumor-microenvironment-responsive biodegradable nano-platform for combination therapy favoring antitumor immune responses. *Nat Commun* 2017;**8**:902.
53. Miller MA, Zheng YR, Gadde S, Pfirschke C, Zope H, Engblom C, et al. Tumour-associated macrophages act as a slow-release reservoir of nano-therapeutic Pt(IV) pro-drug. *Nat Commun* 2015;**6**:8692.
54. Chen Q, Wang X, Wang C, Feng L, Li Y, Liu Z. Drug-induced self-assembly of modified albumins as nano-theranostics for tumor-targeted combination therapy. *ACS Nano* 2015;**9**:5223−33.